# Non-destructive Assessment of the Porosity in Silver (Ag) Sinter Joints using Acoustic Waves

Sebastian Brand[1], Bianca Böttge[1], Michael Kögel[1], Falk Naumann[1], Jurrian Zijl[2], Sebastiaan Kersjes[2], Thomas Behrens[3] and Frank Altmann[1]

[1] Fraunhofer Institute for Microstructure of Materials and Systems, IMWS, Halle, Germany
[2] BESI Netherlands, B.V., Duiven, The Netherlands
[3] Infineon Technologies AG, Regensburg, Germany
Sebastian.Brand@IMWS.Fraunhofer.de

***Abstract*—Caused by its superior performance regarding bandwidth, power loss and form factors compound semiconductors like GaN or SiC recently moved into the interest of the semiconductor industry, particularly for applications in the high power segment. These improved performance parameters go along with increased power densities and thus, require a specifically optimized thermal concept of the packaging. Ag-sintering as die-attach process has been widely accepted as a promising alternative to soldering techniques with respect to thermal conductance. However, the thermal and the mechanical behavior of the sinter layer is influenced by its composition on the micro- and the macroscopic scale with respect to the presence of voids, inclusions and delamination but also the fractional content of porosity. Scanning acoustic microscopy (SAM) uses acoustic waves that interact with the mechanical properties of the sample materials and is thus, widely established for the non-destructive detection of voids, inclusions and delamination in microelectronic components. The current paper investigates the potential of SAM as a method for the assessment and characterization of the porosity in sintered Ag layers targeting the die-attach technology for novel power semiconductor devices.** *(Abstract)*

***Keywords: acoustic microscopy; silver sinter, Ag-joints, die-attach for power electronics***

## I. INTRODUCTION

With the availability of novel semiconductor materials and the increasing power and efficiency demands for conventional Si-based systems, integration, encapsulation and housing of electronic components and systems become increasingly important. Compound semiconductor materials with wide band-gaps and the related higher electron mobility offer superior performance parameters including breakdown voltage, an allowance of higher operation currents, and a significant increase in the switching frequencies at reduced channel resistances [4]. Besides elevated temperatures in high power applications of conventional Si-based semiconductors junction- and ambient temperatures may further increase due to a higher temperature-tolerance of compound semiconductors (SiC) attracting applications in the category of harsh environmental conditions. Since the majority of aging phenomena are accelerated by temperature an increased tolerance to this parameter leads to longer life times and thus, a higher reliability. This on the other hand will act as enabler for specific markets like e-mobility and automotive applications, but also for harsh environments. Besides the semiconductor itself also the packaging needs to be adapted to the altered thermal conditions, as it impacts the reliability and life time at the system and / or module level. The die-attach technology represents a major challenge in the thermal concept for system integration as it thermally, mechanically and electrically interconnects materials with highly differing coefficients of thermal expansion (CTEs) and is exposed to high temperatures and temperature gradients. Soldering, as the conventional die-attach technology in low- and medium power applications is not sufficiently suited for the high power sector. Its mechanical properties, particularly the creeping behavior of solder leads to degradation and finally the formation of cracks and delaminations. Thus, solder joints represent a significant risk for both reliability and life time in high power systems. Joints formed by sintered Ag exhibit a superior behavior over solder when exposed to large temperature gradients and high absolute temperature values. Ag does not tend to creep under cyclic thermal and mechanical loads and remains highly stable over an extended period of repetitive thermal loads with large gradients. However, the process of silver (Ag)-sintering can be very complex and is impacted by a high number of atmospheric and ambient parameters during the sinter sequence that may result in uncontrolled interface failure, which is currently under research. The availability of appropriate characterization techniques would lead to a broader acceptance of Ag-sintering and likely enable applications in "high-reliability" segments like automotive and "harsh environments" but also other consumer and industrial fields. Therefore, techniques that allow for sufficient characterization and corresponding

2377-5726/18/$31.00 ©2018 IEEE
DOI 10.1109/ECTC.2018.00279

equipment for the in-line inspection of Ag-sinter joints are highly desired. Potential applications for metallic sinter joints are of great interest to the emerging and growing market of the e-mobility, power storage, smart grid and renewable energies.

Scanning acoustic microscopy (SAM) is a widely established non-destructively operating method for assessing quality related parameters like the presence of void-, inclusion- and delamination defects in a large number of fields and particularly in microelectronics manufacturing processes. Although it is a widely accepted technique it is mainly used for pure qualitative imaging and quantitative parameters that may be extracted are almost exclusively size-related and are obtained from recorded scan-images. The ability of acoustic waves to extract elasticity related material parameters remains largely unused, even though it forms the fundamental contrast mechanism of the method. The current study investigates the potential of focused acoustic waves to characterize the porosity of sintered Ag-layers as relevant parameter of the die-attach thermal, mechanical and thermo-mechanical properties.

## II. Theory of the Acoustic Approach

Since acoustic waves are mechanical waves that interact with the mechanical properties of the medium of propagation they get reflected, refracted and/or scattered when encountering boundaries between differing materials. In the simplified case of normal incidence and infinite boundaries the reflectivity of an interface between adjacent materials can be expressed by:

$$R(90°) = \frac{Z_2 - Z_1}{Z_1 + Z_2} \quad . \qquad (1)$$

With the reflection coefficient R, the acoustic impedance of the material the wave is coming from $Z_1$, and $Z_2$ denoting the acoustic impedance of the material the wave is propagating to. However, when objects become smaller and reach dimensions near or below the wavelength of the acoustic wave the propagation behavior becomes more complex and the incident acoustic wave is partially scattered in both the forward and backward direction. In the case of an Ag-sinter layer with poresizes in the 1 – 5 µm range and an acoustic wave with wavelength $\lambda = 22$ µm ($v_{Ag} = 3794$ m/s [3], $f_{ac} = 175$ MHz) partial scattering will occur in all spatial directions based on the pore-size, the size distribution and the volume fraction within a resolution cell of the acoustic transducer, likely allowing for the assessment of porosity variations. Additionally, the presence of pores with dimensions below the acoustic wavelength will also alter the bulk values of the mass density and the elastic coefficients which define the acoustic wave propagation. Considering that the velocity $v$ of an acoustic wave depends on both of the above mentioned parameters, any alteration of either one will result in a change of the wave velocity and thus the propagation time. The relationship between the wave velocity and the mechanical material properties is provided in eqn. 2.

$$v = \sqrt{\frac{c_{ij}}{\rho}} \qquad (2)$$

With $c_{ij}$ representing the mode-relevant elastic coefficient (longitudinal wave modulus for a compressional wave or shear modulus for a transverse wave) and ρ the mass density. The time delay between two acoustic echoes that are originated at two adjacent interfaces corresponds to the propagated distance (measurement in impulse-echo mode leads to the factor of 2) and the wave velocity, according to eqn. 3

$$t = \frac{2s}{v} \qquad (3)$$

Here $t$ represents the time of flight (ToF) of the acoustic wave required for traveling to and from the interface (impulse-echo measurement), $s$ the length of the propagation path (thickness of the sinter layer) and $v$ the sound velocity, according to eqn. 2.

An increase in porosity will lead to a decrease in both, the value of the elastic coefficient and the mass density. If the elastic property drops faster with increasing porosity then, according to eqn. 2, the velocity of the acoustic wave should decrease with increasing porosity. Another parameter for describing the acoustic wave propagation and in particular the behavior at boundaries

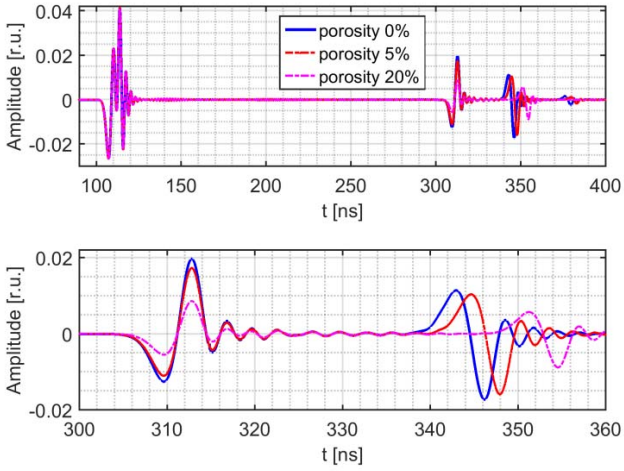


Figure 1: Results of the numerical simulation of the acoustic wave propagation. Top: Acoustic signal of the all sound-material interface interactions inside the sample, computed for a content of 0 %, 5 % and 20 % of porosity in the sinter layer. Bottom: Magnification of the echoes at the interfaces “die / sinter layer” and “sinter layer / substrate”. In conclusion: an increased pore-content results in a decreased reflectivity at the “die / Ag-sinter layer” interface and an increased propagation time (decreased sound wave velocity) in the sinter layer.

between materials of differing mechanical properties is the acoustic impedance (see eqn. 1). It is defined as the ratio of traction to particle displacement velocity [3]. It can however, also be expressed as:

$$Z = \rho v \tag{4}$$

With $Z$ denoting the acoustic impedance, $\rho$ the mass density and $v$ the sound wave velocity. Substituting $v$ in eqn. 4 by eqn. 2 leads to:

$$Z = \sqrt{c_{ij}\rho}\,, \tag{5}$$

expressing that the acoustic impedance of the porous medium decreases with increasing porosity. Considering the material combination of the samples investigated in the current study reveals that the Ag of the sinter layer has an acoustic impedance of 39.84 MRayl while Z of the Si-die is 19.64 MRayl according to [3]. An increase in porosity in the sinter layer will result in a larger volume fraction of gas in the Ag. As a consequence an increase in porosity of the sinter layer will adapt its acoustic impedance towards the value of the Si-die which results in a smaller gradient of the acoustic impedance ($Z_2 - Z_1$) and, according to eqn.1, decrease the reflectivity of the interface Si/Ag. Meanwhile, the propagation time in the sinter layer will increase as the acoustic wave velocity decreases according to the eqns. 2 and 3.

Figure 1 shows the results of numerical simulation of the acoustic wave propagation. The top-graph shows the acoustic signal with the echoes from the entrance into the Si-die, the interaction at the interface Si-die / sinter layer and the interface sinter material / substrate. The simulations were performed for compact Ag, Ag with 5 % porosity and Ag with 20 % porosity using PZFlex (PZFlex, Weidlinger Ass., CA, USA). The bottom-graph in fig. 1 shows an enlargement of the echo signal in the time range between 300 ns to 360 ns, magnifying the echoes obtained from the interfaces Si-die / sinter layer and sinter layer / substrate for all three material compositions of the sinter layer. The echo from the interface Si-die / Ag-sinter layer shows a strong dependency between its amplitude and the porosity of the sinter material. The reflectivity at this interface decreases with increasing pore-content since, as elaborated above, the effective acoustic impedance of the sinter layer also decreases, leading to a reduced gradient between the Si-die and the Ag-sinter layer. Additionally, the results of the simulation contained in fig. 1 show that the propagation time of the acoustic wave increases with increasing pore-content, supporting the hypothesis described above. As the results obtained from the modelling and numerical simulation agree well with the theoretical considerations made here, it needs to be mentioned that the effect that small variations in the porosity induce on the acoustic signal may easily be shadowed by the influence of larger variations in the material properties, their homogeneity and the presence of defects.

In summary the current hypothesis assumes that an increase in porosity is expected to be accompanied by 1st : an increase in the ToF of the acoustic wave in the sinter layer, 2nd: a decrease of the reflectivity of the Si-die / Ag-layer interface and 3rd : an increase in the scattered energy from within the Ag-layer.

## III. Materials and Methods

### A. Sample Description

For each sample, 12 Si-dies were sintered on one direct copper bonded (DCB) substrate (Curamic Power Plus Boards, Roger Corporation, CA, USA). The Si-dies had a size of 8 mm x 8 mm, a thickness of 250 µm and were metalized by 50 nm Ti, 100 nm Ni and a 1 µm Ag-finish. The DCB substrate consisted of alumina ($Al_2O_3$) metallized with 300 µm Cu on both sides and coated with 650 nm of Ag. Henkel Electronic Materials provided a Ag-sintering paste running in volume production. The paste has an Ag-content larger than 85% with easy and consistent stencil printing performance. Sample preparation started by cleaning the DBC boards in a plasma oven. After that, by means of a manual screen printing process, a Ag-paste layer of 80 µm thickness was applied on the DBC board. After printing, the Ag-paste layer was allowed drying in an oven at 120°C for 40 min. The Si-dies have then been placed manually on the dried Ag-paste layer. Finally, the prepared DBC samples were placed in a steel carrier to be placed in the sinter machine. The sintering itself was performed in a manual hot press (250°C) with a sacrificial PFA foil of 125 µm thickness acting as protection buffer between the Si-die and the sinter tool. The press consisted of two flat plates with the prepared samples in between. During placement of the samples, the steel carrier was not in contact with the press to avoid substantial preheating effects of the Ag-paste. The sintering is performed at a clamping pressure of 11 MPa which is achieved prior to the samples being heated thoroughly. The pressure was kept constant at 11 MPa throughout the intended sinter period which here varied between 5 s and 180 s.

### B. Acoustic Microscopy

The sinter layers were inspected non-destructively using a conventional scanning acoustic microscope (SAM 400, PVA TePla AS, Westhausen, Germany). The SAM was equipped with a focused 175 MHz transducer with a focal length of 5.9 mm (in water). Broadband electrical excitation was applied to the ultrasonic probe to obtain short acoustic pulses and thus to enable inspection and evaluation of the sinter layer. For impedance matching

de-ionized and degassed water @ 21 °C was used as coupling fluid between the acoustic lens and the sample. Acoustic data acquisition was performed in C-mode by scanning the transducer across the surface of the sample and received signals were digitized at a rate of 1 GS/s with a resolution of 8 bit by the SAMs internal AD-converter and stored for off-line signal analysis. Signal processing was then conducted using the MATLAB- (The Mathworks, Nattick, MA, USA) based SAMnalysis software toolbox developed in-house. From the ultrasonic echoes several energy related signal parameters (BAI, SSP) [1, 2] were computed within a specified time gate that corresponded to the sinter-layer and used for forming parametric images. From the SAM data also acoustic cross-sections (B-Scans) have been extracted for investigating the Time-of-Flight (ToF) of the acoustic waves inside the sinter layer.

### C. *Physical preparation, microstructure and morphological analysis*

For investigating and analyzing the microstructure of the Ag-sinter layer and the morphology of the pores, scanning electron microscopy (SEM) imaging on cross sections of the sinter layers has been performed. For physical preparation the samples have been embedded in epoxy resin and prepared in cross section by several mechanical grinding and polishing steps. To obtain an excellent surface quality without smearing artefacts caused by the softness of the Ag, samples received a final preparation step by ion-polishing using a JEOL cross section polisher (JEOL GmbH, Freising, Germany). Following this preparation high resolution imaging of the microstructure was performed by SEM using a Zeiss Supra-55 VP (Carl Zeiss Microscopy GmbH, Oberkochen, Germany).

From the electron micrographs the porosity was approximated using image analysis software developed in-house in MATLAB (The Mathworks, Nattick, MA, USA). The software performed object identification upon thresholding and segmentation. Parameters extracted from the electron micrographs were the number of pores, the pore sizes, the mean-equivalent diameter, and the axis ratios of ellipsoidal approximation.

## IV. Results and Discussion

The aim of the current study is the fundamental theoretical and experimental investigation of the potential of acoustic waves for the assessment of the porosity in sintered metal layers. According to the theoretical consideration made above modelling and numerical simulation was performed. In the model the values of the mass density and the elasticity of bulk Ag were adjusted to mimic alterations in the porosity of the sinter material between 0% and 20%. The results of the numerical simulation study were in concordance with the

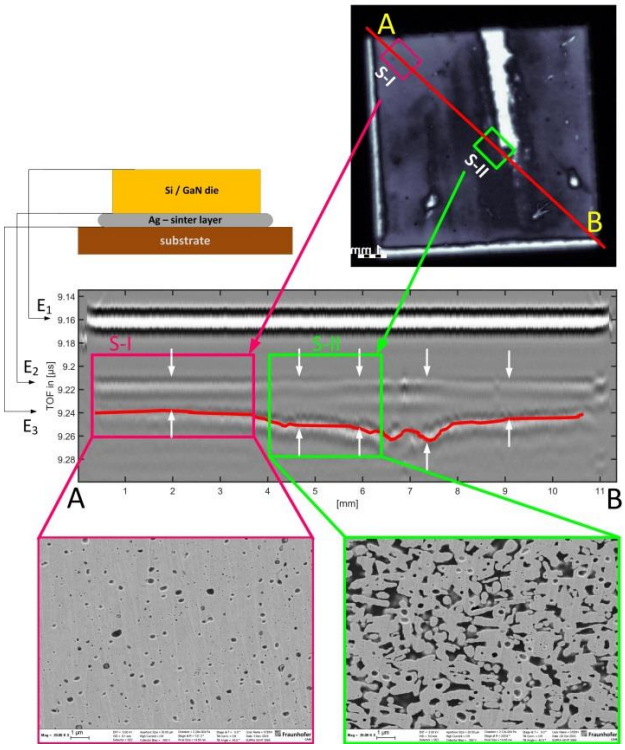


Figure 2: Results of acoustic and microstructural analysis on Ag-sintered samples. Upper-left: schematics of the sample in cross-section with indication of the interfaces and the acoustic echoes. Upper-right: acoustic micrograph at the interface Si-die/Ag-sinter layer. Vertical-center: acoustic cross-section along the red-line-marker in the acoustic micrograph from A to B. Bottom: electron micrographs of the sintered Ag-layer at the locations labelled "S-I" and "S-II" in the acoustic micrograph and the acoustic cross-section, showing a variation in the porosity.

theoretically expected behavior of the acoustic waves with respect to the interface reflectivity at the interface Si-die / Ag-sinter layer and the wave velocity of the compressional wave in the sinter material, as shown in fig. 1. Here the propagation time in the Ag-layer increases with increasing porosity while the reflectivity at the interface Si-die/Ag-layer decreases. Figure 2 shows an acoustic micrograph (upper-right image) of a sample containing an inhomogeneous sinter layer. The SAM image represents the acoustic energy at the interface Si-die / Ag-layer of the sample. Thus, regions with higher intensity, corresponding to a higher acoustic energy, should indicate a lower porosity. The white area in the acoustic image corresponds to a delamination, where the incident acoustic wave is fully reflected leading to a high signal energy of this echo. A schematic of the sample (upper-left image in fig. 2) illustrates the interfaces and the materials involved. In the vertical center of fig. 2 an acoustic cross-section, a so called B-scan, through the

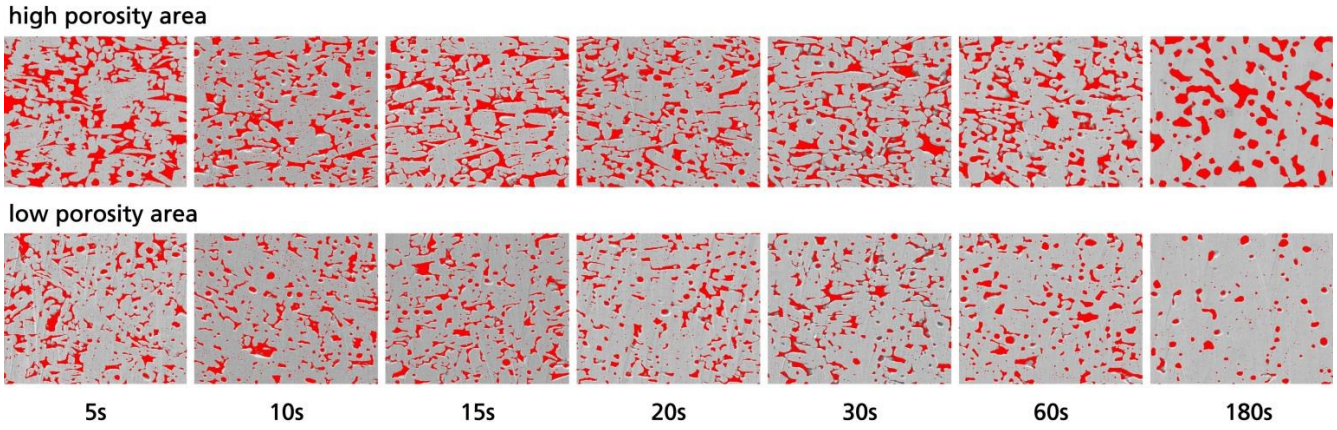


Figure 3: Processed electron micrographs of the physical cross-sections of the Ag-layers as a function of the sinter time. The upper row was recorded at areas where the acoustic micrograph showed a decreased intensity as indicated by S-II in figure 2 (which was expected to correspond to a high porosity). The bottom row was obtained in areas of the sample where a lower porosity was concluded (as indicated by S-I in figure 2). A decrease of the pore content is visible for both locations at increased sinter duration between 5s and 180s.

sample is shown. The arrows labelled $E_1$, $E_2$, and $E_3$ connect this acoustic cross-section to the sample structure and indicate the corresponding interfaces. The trace of the echo $E_3$ has been marked by a red line to pronounce its irregular shape. From the B-scan, it can be seen that the echo intensity of echo $E_2$, which corresponds to the interface Si-die/Ag-layer, has a higher intensity in the region labelled S-I (magenta - colored) compared to the area S-II (green). In addition, the ToF between the echoes $E_2$ and $E_3$ is larger in the spot S-II compared to S-I. According to the hypothesis made in the theory section of this paper, the porosity in the area S-I should be lower and thus the Ag-layer should be more compact than in the area S-II. Physical cross sections have been prepared at the locations labelled S-I and S-II and were investigated at high resolution by SEM. At the bottom of fig. 2 two electron micrographs show the microstructure of the Ag-layer at the locations S-I and S-II. In agreement with the theoretical considerations the more compact and less porous structure of the Ag-layer corresponds to the region where the higher acoustic energy (higher reflectivity) at the interface Si-die / Ag-layer is obtained. The lower reflectivity at the Si-die / Ag-layer interface and lower sound velocity however,are observed in the area of higher porosity. These results indicate the susceptibility of acoustic waves for the material alterations induced by a structure with physical dimensions way below the wavelength of the insonated acoustic waves. Considering an acoustic frequency of approx. 175 MHz in Ag with a sound velocity of $v \approx 3794$ m/s the wavelength is $\lambda \approx 22$ µm at best, neglecting frequency downshift effects caused by acoustic attenuation. With pore dimensions in the 1 µm regime and considerably below the structural dimensions of the "inclusions" that impact the reflectivity and propagation of the acoustic waves can be less than $\frac{1}{50}$ th of the wave length. It, however, seems unlikely that a structure with such a large fraction of the physical dimension, compared to the wavelength, leads to such a significant impact on the acoustic wave. It is therefore concluded, that it are rather the effective values of the elastic coefficients and the mass density which alter the "bulk properties" of the sinter material, which is encountered by the acoustic waves.

Following these fundamental investigations that illustrate the principal ability of acoustic waves to detect material variations caused by porosity the sensitivity to changes in the porosity need to be addressed. To obtain samples with decreasing pore content in the Ag-sinter layer identical samples were prepared but sintered for decreased durations. Otherwise sinter parameters were kept constant to avoid further influence on the sinter layer. Samples were sintered as described for 5s, 10s, 15s, 20s, 30s, 60s and 180s. It has been observed from previous studies and practical experience that the majority of the morphological changes in the sinter material occur in the first 30-60 s of sintering and that the relative porosity changes considerably within that time. The samples have been investigated by SAM and acoustic signals were recorded and stored for off-line analysis. Following the acoustic inspection samples were cross-sectioned and investigated by SEM. For assessing the porosity SEM-images were analyzed using an in-house developed image analysis software. Figure 3 shows the electron micrographs of the physical cross sections. For illustration purposes pixels which were detected as pore-related are indicated red and are superimposed on the electron micrographs. From fig. 3 it is difficult to pinpoint the morphological changes along the sinter period. However, a decrease in the porosity between the samples sintered for 5s and for 180s is noticeable. From the SAM

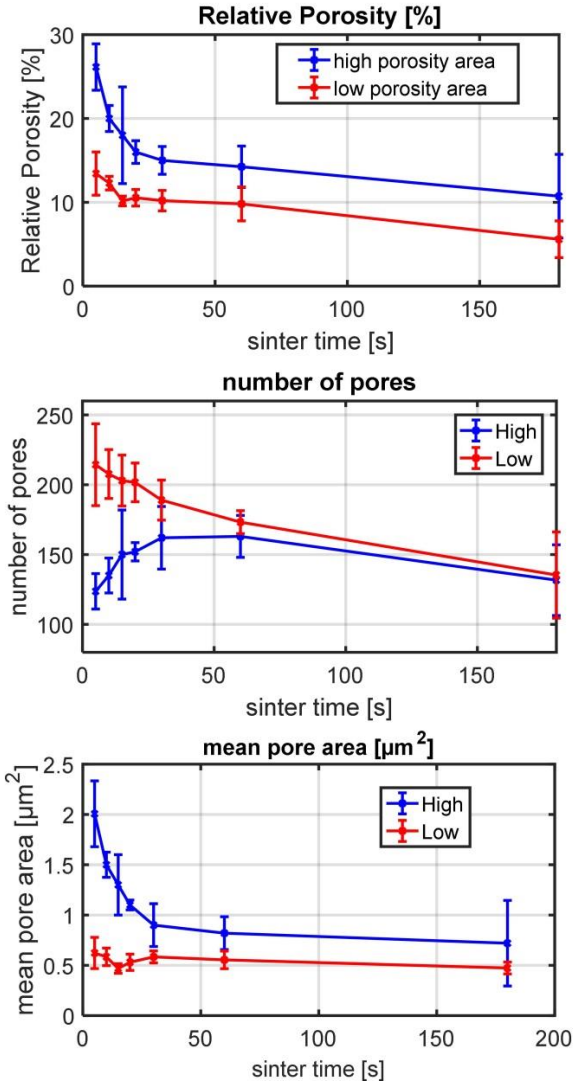


Figure 4: Results of the morphological analysis of the electron micrographs using the custom developed software. Top: At low sinter durations the relative porosity is high and decreases with sinter time. Center: The number of pores is higher in the low-porosity area and converges towards a final value which is similar to the one of the high-porosity area. Bottom: The average cross-sectional area of the pores in the low-porous area is lower over the entire sinter sequence. In both areas the pore cross-section decereases as the sinter duration increases.

investigation it was observed that the sinter layers formed also showed an inhomogeneity, as observed in the sample shown in fig. 2. This offered the opportunity to not only investigate inter-sample changes in porosity but also variations that occur within a sample and which are expected to be much smaller than in between the samples. From each of the samples two physical cross sections were prepared and are shown in fig. 3. Electron micrographs of areas with lower signal energy of the echo Si-die / Ag-layer are shown in the upper row while the bottom row contains SEM images of locations where the

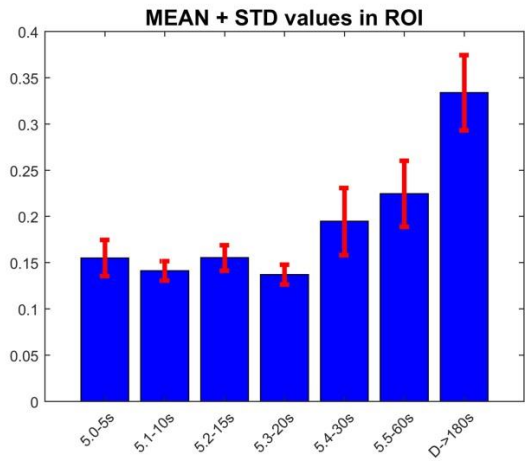


Figure 5: Mean and standard deviation of the signal energy after normalization to the entrance echo into the Si-die. The normalized signal energy increases with sinter duration and thus agrees with the theoretical considerations.

acoustic signal had a higher intensity at the same interface. For illustration purposes all pixels that were detected to be pore-related are indicated red in the graphs in fig. 3. Considering the first (left-most) and the last (right-most) samples of the sinter sequence a decrease in the porosity can be observed. It can also be seen from fig. 3 that the pore content in the sinter layer is lower in the bottom row compared to the top-row. The results of the morphological investigation of the sinter layers' microstructures by analyzing the SEM images are shown in fig. 4. Here the relative porosity, the normalized number of pores and the area of the cross section of the individual pores are shown. To obtain statistical information and thus information of the robustness and reliability of the estimates multiple regions of interest (ROI) were analyzed from each cross section (multiple SEM images were recorded and analyzed). From the estimates the mean values and their corresponding standard deviations are plotted in fig. 4. It can be noticed from fig. 4 that the normalized number of pores is larger in areas of lower porosity in earlier sinter stages. However, the mean pore diameter is considerably lower in the low-porosity regions of the cross sections. It is noticeable that the normalized number of pores converges to a similar value for both regions as the sinter process continues. In the high-porosity area the total number of pores is smaller at the beginning of the sinter process but pores are drastically larger and remain larger as in the lower porosity area, which results in a higher porosity value. The authors do acknowledge the paradox of estimating pore sizes from cross sections. However, when analyzing the electron micrographs in fig. 3 at least two facts can still be observed reliably. The first is that the morphology of the pores changes over the sinter process and that pore cross sections form more circular with

increasing sinter duration. The second fact that can be observed is the higher spatial frequency and thus that the rate of the pores is higher at the beginning of the sinter process versus the end, but also in the high-porosity area compared to locations of lower porosity.

For the acoustic analysis compensation of the systems transfer characteristics was required to be compensated for. All acoustic data were normalized in time domain to the amplitude of the entrance echo into the Si-die. This was considered to be valid as the adjacent materials, de-ionized and degassed water @ 21 °C, and mono-crystalline Si for electronic applications is highly investigated and can be assumed rather constant in their acoustic properties. This normalization process allowed for comparable results throughout the individual signals and acoustic micrographs of the study. For correlation the energy of the echo obtained from the interface Si-die / Ag-layer was estimated. Also, in order to obtain a statistics, values were estimated from multiple ROIs and mean values and their standard deviations have been computed. The results of the acoustic analysis are shown in fig. 5. Figure 5 also shows that the acoustic energy at the Si-die / Ag-layer interface is rather low and stable in the beginning of the sinter process, when the porosity is rather high. After 30 s of sintering the acoustic energy and its standard deviation at the interface Si-die / Ag-layer increases allowing the assumption of a higher randomness of the pores and smaller effective pore sizes with a decreased overall porosity. As the sinter process continues

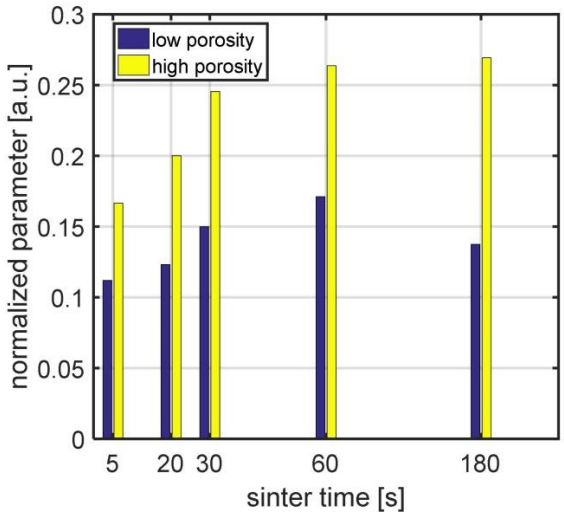


Figure 6: Preview on the acoustic signal analysis with inclusion of the sound wave velocity. Acoustic signals were normalied in intensity onto the interface echo water / Si-die to compensate for systematic and imaging variations. The ToF inside the sinter layer was included in the normalized parameter. Here the increase in both parameters with sinter time is visible and a differentiation between high- and low-porous regions is possible. The ToF was not compensated for thickness variation of the Ag-layer.

the mean energy of the interface echo increases which is in agreement with both the theoretical expectations and the results of the morphological analysis shown in the figs. 3 and 4. However, the results in fig. 5 only represent the effect the porosity inflicts on the reflectivity at the interface between the Si-die and the Ag-sinter layer. The acoustic energy does not account for the variation of the acoustic wave velocity which is induced upon an alteration of the porosity, as elaborated in detail in section II. However, the samples investigated in the current study were semi-manually processed, as they could not have been taken from a manufacturing line. As a consequence the thicknesses of the sinter layers were not perfectly constant. In theory this deviation could be accounted for as an acoustic inspection offers the ability to measure absolute and relative distances if the sound velocity is known. In the present study this however, was not performed and is a potential topic of future work. When careful compensation of thickness variations is performed the acoustic wave velocity can be estimated and incorporated into an analysis algorithm for quantitatively estimating the porosity of Ag-sinter layers. Figure 6 gives a preview of the correlation of a combined reflectivity- and wave velocity- related acoustic parameter to the porosity of the Ag-layer. The combined parameter of reflectivity and wave velocity plotted in fig. 6 shows a clear correlation to the porosity as a function of the sinter time. Besides, also a differentiation between regions of high- and low-porosity seems possible in fig. 6.

## V. Conclusion and Outlook

Acoustic microscopy in combination with signal analysis has been successfully performed on Ag-sinter layers intended as the die attach for power electronic devices. To investigate the sensitivity of acoustic waves to variations in the sinter porosity with pore sizes significantly below the resolution capabilities physical cross section preparation in combination with high-resolution SEM analysis of the microstructure of the samples was performed. From recorded electron micrographs the porosity and the morphology of the pores of the sinter layers were estimated. Results of the morphological analysis and the acoustic analysis were correlated and showed good agreement. The experimental results obtained are in accordance with the theoretically expected relationship between the sinter-layer porosity and the acoustic properties reflectivity and sound wave velocity. It was observed that the majority of the morphological changes occur in the first 30-60 s of the sinter process which supported previous experience. The shape of the pores change from an elliptical at the beginning, to a rather circularly shaped cross section at the end of the sinter process. The observations obtained in the current study suggest a high sensitivity of acoustic waves for the assessment of the porosity in Ag-sinter layers. Future work should address a more rigorous compensation of

variations in the thickness of the layers and potential sample tilt. However, it should also be mentioned that larger structural or parametric deviations like inclusions or layer delamination will impact and falsify the porosity estimates. However, that would be an exclusion criterion in itself, which would not negatively impact the false-positive classification rate of an inspection tool.

## VI. ACKNOWLEDGEMENTS

The project “PowerBase” has received funding from the Electronic Component Systems for European Leadership Joint Undertaking under grant agreement No 662133. This Joint Undertaking receives support from the European Union’s Horizon 2020 research and innovation program and from Austria, Belgium, Germany, Italy, Netherlands, Norway, Slovakia, Spain and the United Kingdom.

## VII. REFERENCES

[1] Raum K, et al. (1998) Channel defect detection in food packages using integrated backscatter ultrasound imaging. *Ieee Transactions on Ultrasonics Ferroelectrics and Frequency Control* 45, 30-40.

[2] Tismer S, et al.(2013) Acoustic Imaging of Bump Defects in Flip-Chip devices using Split Spectrum Analysis. Proceedings of the 2013 IEEE Ultrasonics Symposium, Praque, Czech. Rep.

[3] Briggs A (1992) 'Acoustic Microscopy, in monographs on the physics and chemistry of materials.' (Oxford University Press: Oxford)

[4] Meneghini M, Tajalli A, Moens P, Banerjee A, Zanoni A, Meneghesso G, Trapping phenomena and degradation mechanisms in GaN-based power HEMTs,Materials Science in Semiconductor Processing, 2017, ISSN 1369-8001, https://doi.org/10.1016/j.mssp.2017.10.009.